

Supporting Information

Ultra-high photoelectric conversion efficiency and obvious carrier separation in a photovoltaic ZnIn_2X_4 (X = S, Se and Te) van der Waals heterostructures

Zheng Liang¹, Yao-Zhong Liu¹, Ze-Ting Gong¹, Jun-Yao Li¹, Yong-Sheng Yao¹, Zhen-Kun Tang^{1*},
Xiao-Lin Wei^{1*}

¹ Key Laboratory of Micro-nano Energy Materials and Application Technologies, University of Hunan Province &
College of Physics and Electronics Engineering, Hengyang Normal University, Hengyang 421002, China

*Email: zktang@hynu.edu.cn, xlw@xtu.edu.cn

Table S1

Calculated lattice constants a/b (Å) of ZIX ($X=S, Se$ and Te) monolayer and its heterostructures. For comparison, the relaxed lattice constants of the previous ZIX monolayer also listed.

Structure	a/b (Å)	a/b (Å, Ref. 39)	a/b (Å, Ref. 40)
ZnIn ₂ S ₄	6.71/3.88	6.78/3.93	6.68/3.87
ZnIn ₂ Se ₄	7.00/4.05	7.09/4.10	7.01/4.06
ZnIn ₂ Te ₄	7.50/4.34	7.63/4.41	7.56/4.37
ZIS/Se	6.86/3.97		
ZISE/Te	7.27/4.20		

Table S2

The calculated bandgap of ZIX monolayer and its heterostructures by PBE, standard HSE06 ($\alpha=0.25$), PBE0, PBE+SOC and HSE06 ($\alpha=0.13$) functional, respectively. For comparison, the previous results were also listed. D and I represents direct bandgap semiconductors and indirect bandgap semiconductors, respectively.

Structure	PBE	HSE06 ($\alpha=0.25$)	PBE0	PBE+ SOC	HSE06 ($\alpha=0.13$)	PBE (Ref. 39)	HSE06 (Ref. 39)	HSE06 (Ref. 40)
ZnIn ₂ S ₄	1.80(D)	2.73(D)	3.53(D)	1.79(D)	2.34(D)	1.79(D)	2.74(D)	3.00(D)
ZnIn ₂ Se ₄	1.24(D)	1.96(D)	2.70(D)	1.13(D)	1.64(D)	1.98(D)	1.98(D)	2.20(I)
ZnIn ₂ Te ₄	0.90(I)	1.54(I)	2.15(I)	0.69(I)	1.22(I)	0.73(I)	1.28(I)	1.42(I)
ZIS/Se	0.95(D)	1.79(D)	2.54(D)	0.62(D)	1.43(D)			
ZISE/Te	0.18(D)	0.84(D)	1.41(D)	0.01(D)	0.49(D)			

Table S3

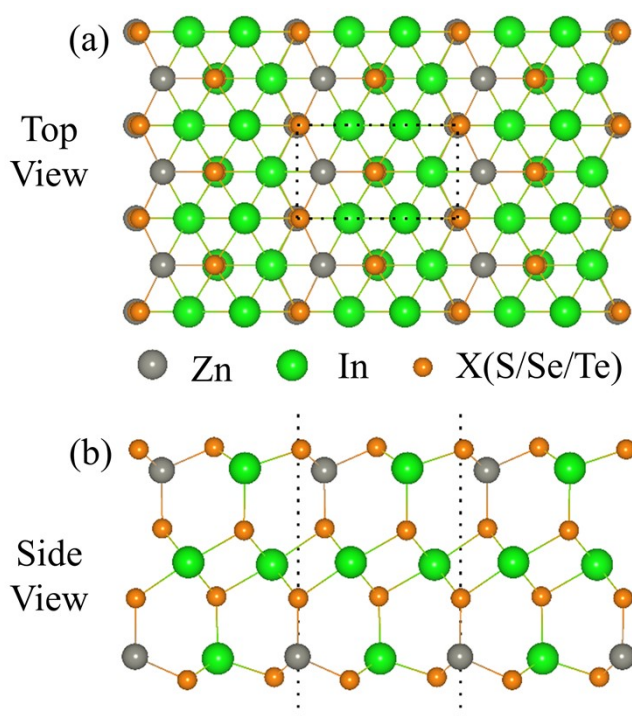
The lattice constant and binding energy E_b of four different types of stacked heterostructures.

Structure	a (Å)	b (Å)	E_b (eV)
ZIS/Se-A	6.86	3.97	-1.46
ZIS/Se-B	6.84	3.97	-1.44
ZIS/Se-C	6.84	3.96	-1.45
ZIS/Se-D	6.85	3.96	-1.28
ZISE/Te-A	7.27	4.20	-1.24
ZISE/Te-B	7.24	4.21	-1.17
ZISE/Te-C	7.26	4.20	-1.23
ZISE/Te-D	7.25	4.19	-0.98
ZIS/Te-A	7.10	4.10	-0.60
ZIS/Te-B	7.09	4.12	-0.56
ZIS/Te-C	7.09	4.10	-0.38
ZIS/Te-D	7.10	4.10	-0.37

Table S4

Electrons and holes effective mass of ZIX (X=S, Se and Te) monolayer and its heterostructures.

Materials	Type of carriers	$m_{\Gamma-X}^*/m_0$	$m_{\Gamma-Y}^*/m_0$	$m_{\Gamma-M}^*/m_0$
ZIS	e	0.247	0.243	0.243
	h	0.365	2.060	1.588
ZISe	e	0.195	0.191	0.191
	h	0.708	1.449	4.257
ZITe	e	0.811	0.263	0.343
	h	2.425	1.857	3.223
ZIS/Se	e	0.180	0.180	0.180
	h	1.811	3.767	2.649
ZISe/Te	e	0.149	0.149	0.148
	h	4.260	0.814	2.018

**Fig. S1** A supercell of ZIX (X=S, Se and Te) monolayer. The gray, blue and orange balls represent the elements Zn, In and X, respectively.

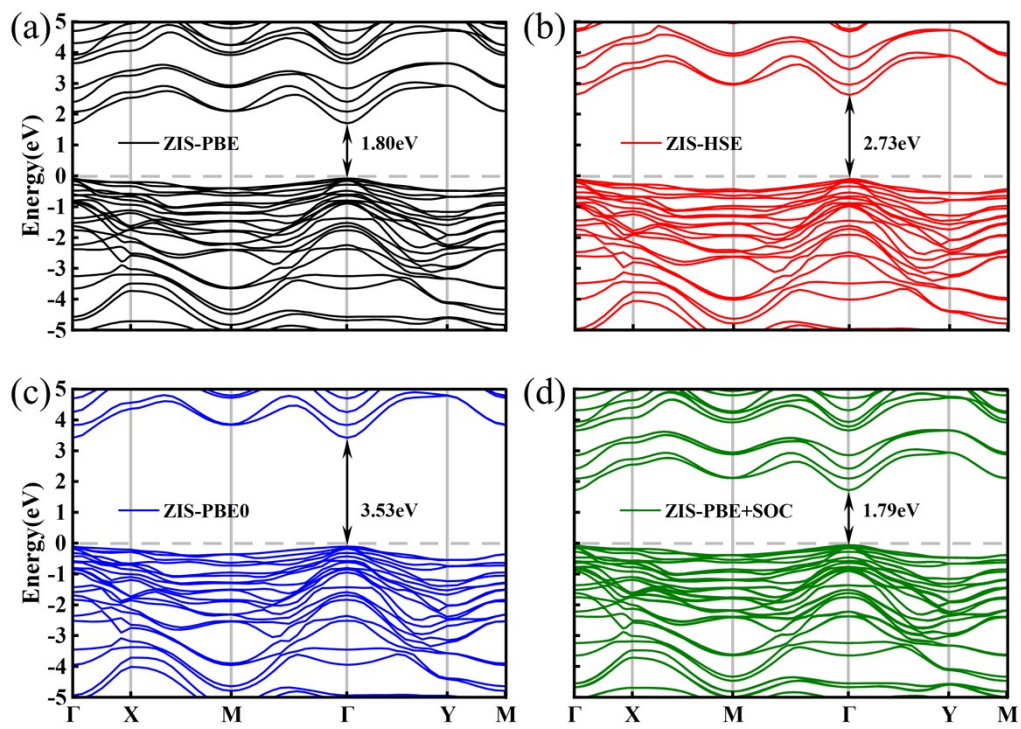


Fig. S2 (a-d) The calculated band structures of ZIS by different functional.

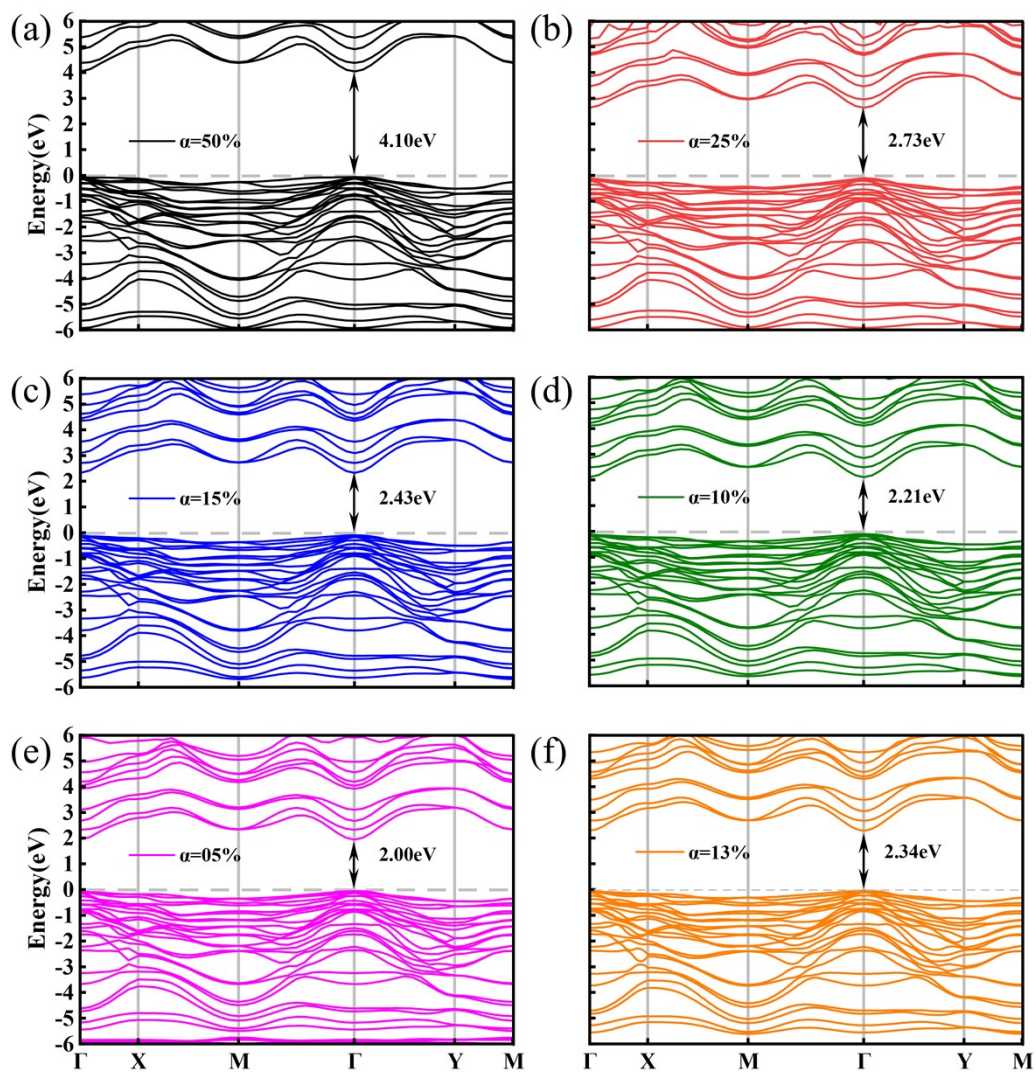


Fig. S3 (a-e) The calculated band structures of ZIS by HSE functional with different mixing ratio.

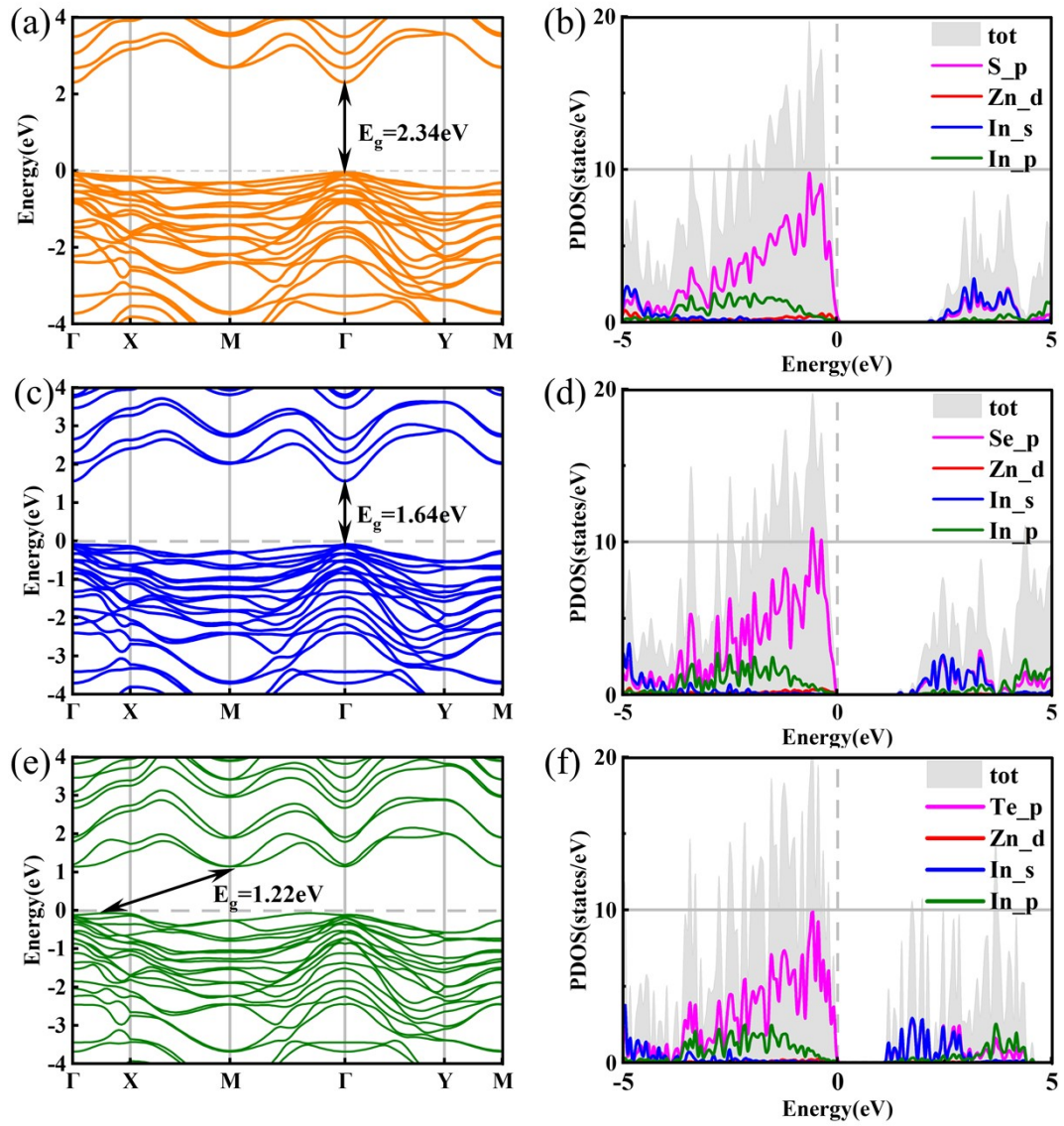


Fig. S4 (a-c) The band structures of ZIS, ZISE, and ZITE monolayer. (d-f) The corresponding density of states (DOS) of ZIS, ZISE, and ZITE monolayer.

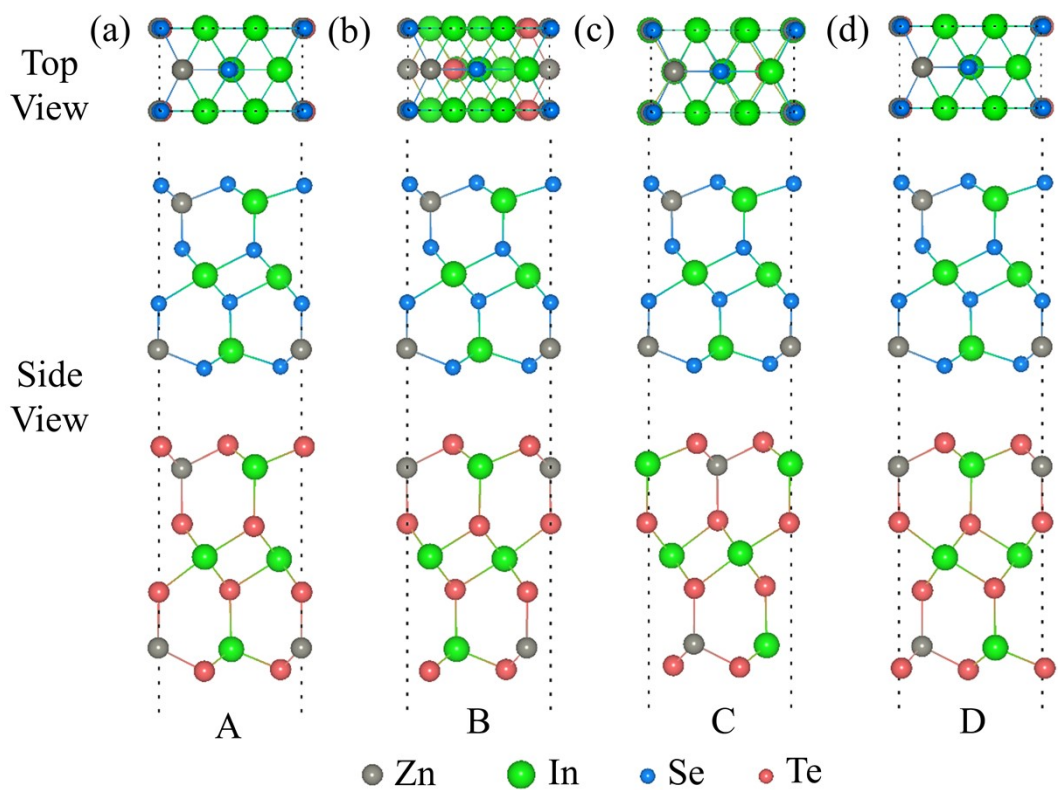


Fig. S5 Top and side views of four different configurations of ZInSe/Te heterostructure. (a) configuration A, (b) configuration B, (c) configuration C and (d) configuration D. The gray, green, blue and red balls represent Zn, In, Se, and Te atoms, respectively.

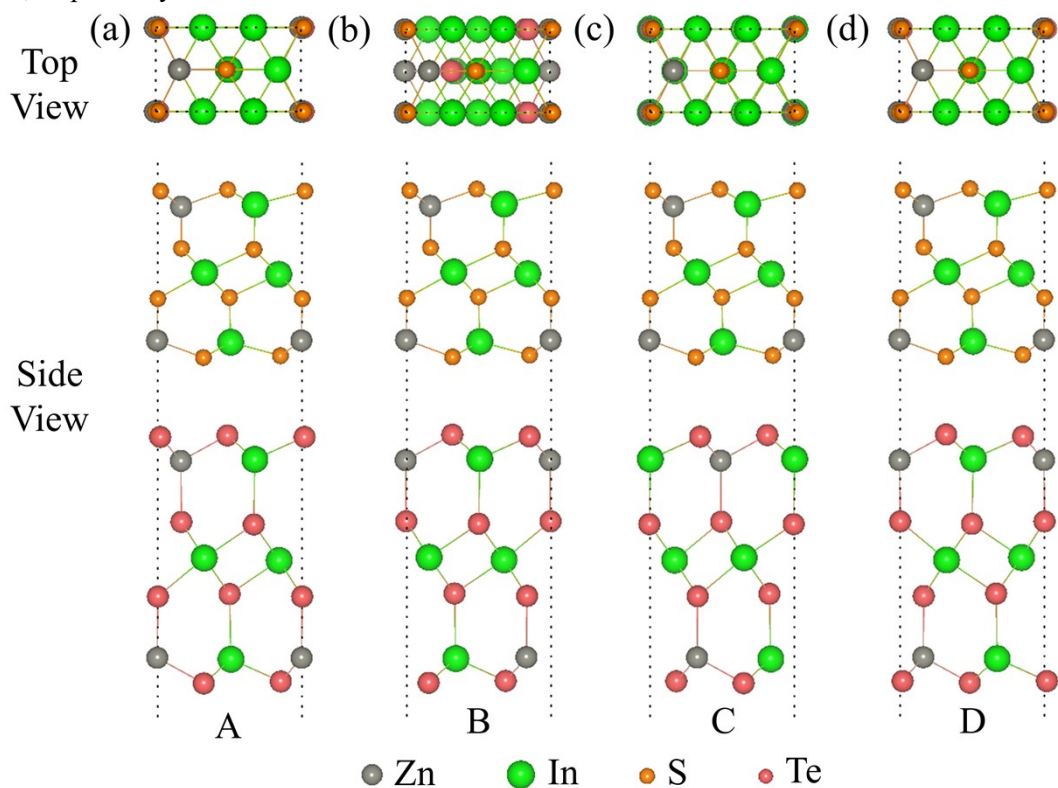


Fig. S6 Top and side views of four different configurations of ZInS/Te heterostructure. (a) configuration A, (b) configuration B, (c) configuration C and (d) configuration D. The gray, green, orange and red balls represent Zn, In, S, and Te atoms, respectively.

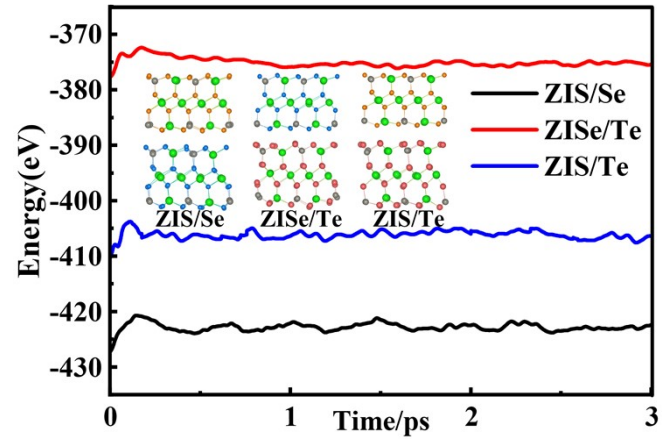


Fig. S7 Energy changes of ZIS/Se, ZISe/Te and ZIS/Te heterostructures at 300 K FPMD simulation. The insets show the final structures after 3000fs FPMD simulation.

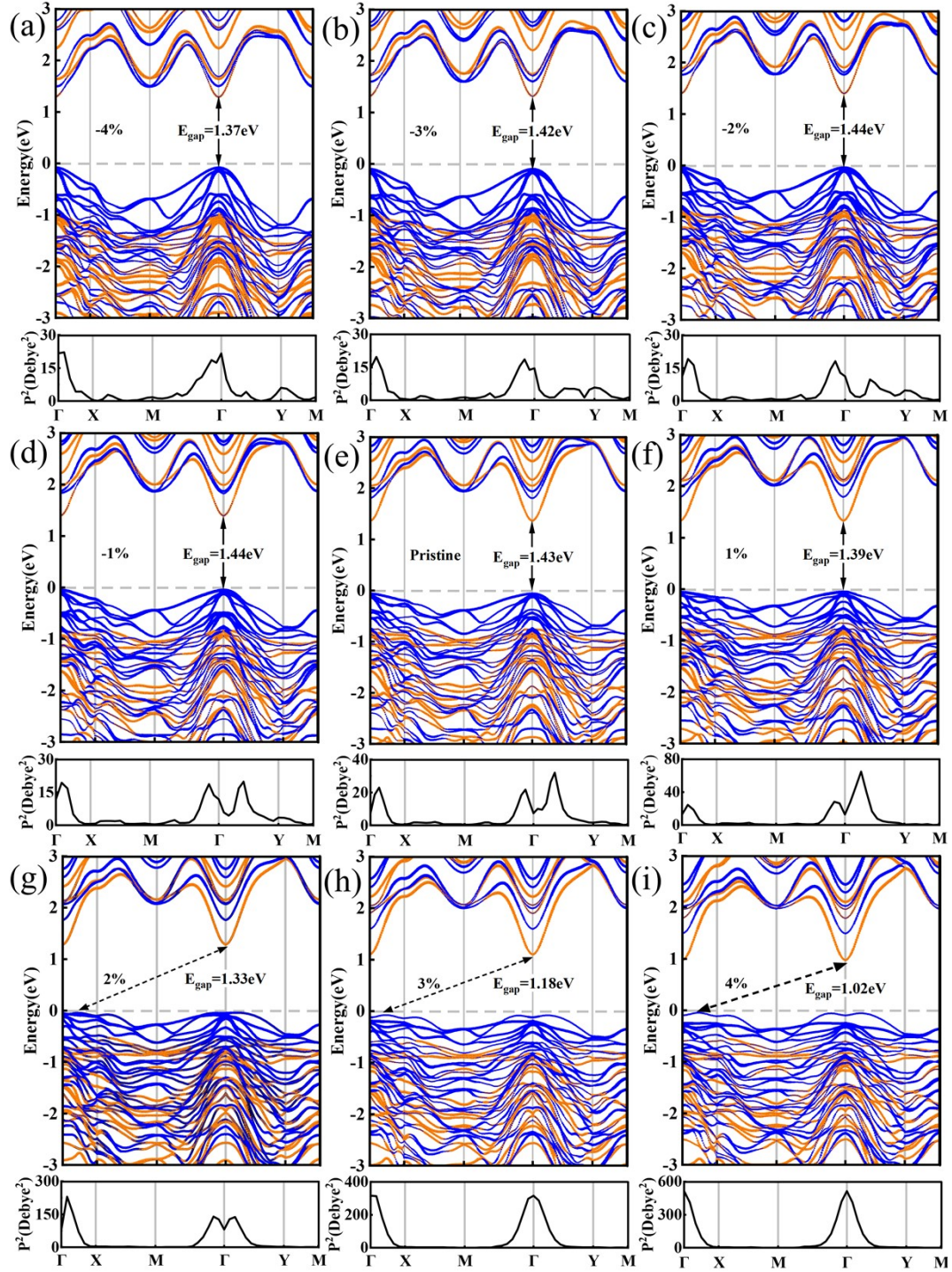


Fig. S8 (a-i) The projected band structures and transition dipole moment (TDM) of ZIS/Se heterostructure under -4% to 4% strains.